Trace elements during primordial plexiform network formation in human cerebral organoids

Rafaela C Sartore [1, 2] , **Simone C Cardoso** [3] , **Yury VM Lages** [1, 2] , **Julia M Paraguassu** [1, 2] , **Mariana P Stelling** [4] , **Rodrigo F Madeiro da Costa** [1] , **Marilia Z Guimaraes** [1, 2] , **Carlos A Pérez** [5] , **Stevens K Rehen** Corresp. [1, 2]

[1] D'Or Institute for Research and Education (IDOR), Rio de Janeiro, Brazil

[2] Institute of Biomedical Sciences, Federal University of Rio de Janeiro, Brazil

[3] Physics Institute, Federal University of Rio de Janeiro, Brazil

[4] Instituto Federal de Educação, Ciência e Tecnologia do Rio de Janeiro, Brazil

[5] Brazilian Synchrotron Light Laboratory, São Paulo, Brazil

Corresponding Author: Stevens K Rehen
Email address: srehen@lance-ufrj.org

Systematic studies of micronutrients during brain formation are hindered by restrictions to animal models and adult post-mortem tissues. Recently, advances in stem cell biology have enabled recapitulation of the early stages of human telencephalon development *in vitro*. In the present work, we analyzed cerebral organoids derived from human pluripotent stem cells by synchrotron radiation X-ray fluorescence in order to measure biologically valuable micronutrients incorporated and distributed into the exogenously developing brain. Our findings indicate that elemental inclusion in organoids is consistent with human brain tissue and involves P, S, K, Ca, Fe and Zn. Occurrence of different concentration gradients also suggests active regulation of elemental transmembrane transport. Finally, the analysis of pairs of elements shows interesting elemental interaction patterns that change from 30 to 45 days of development, suggesting short- or long-term associations, such as storage in similar compartments or relevance for time-dependent biological processes. These findings shed light on which trace elements are important during human brain development and will support studies aimed to unravel the consequences of disrupted metal homeostasis for neurodevelopmental diseases, including those manifested in adulthood.

Trace elements during primordial plexiform network formation in human cerebral organoids

Rafaela C. Sartore[1,2], Simone C. Cardoso[3], Yury M. Lages[1,2], Julia M. Paraguassu[1,2], Mariana P. Stelling[4], Rodrigo F. Madeiro da Costa[1], Marilia Z.P. Guimarães[2], Carlos A. Pérez[5], Stevens K. Rehen[1,2*]

[1]D'Or Institute for Research and Education (IDOR) · Rio de Janeiro · Brazil
[2]Institute of Biomedical Sciences · Federal University of Rio de Janeiro · Brazil
[3]Physics Institute · Federal University of Rio de Janeiro · Brazil
[4]Instituto Federal de Educação, Ciência e Tecnologia do Rio de Janeiro · Brazil
[5]Brazilian Synchrotron Light Laboratory · São Paulo · Brazil

* Corresponding Author: Stevens Rehen

Email: srehen@lance-ufrj.org

Abstract

Systematic studies of micronutrients during brain formation are hindered by restrictions to animal models and adult post-mortem tissues. Recently, advances in stem cell biology have enabled recapitulation of the early stages of human telencephalon development *in vitro*. In the present work, we analyzed cerebral organoids derived from human pluripotent stem cells by synchrotron radiation X-ray fluorescence in order to measure biologically valuable micronutrients incorporated and distributed into the exogenously developing brain. Our findings indicate that elemental inclusion in organoids is consistent with human brain tissue and involves P, S, K, Ca, Fe and Zn. Occurrence of different concentration gradients also suggests active regulation of elemental transmembrane transport. Finally, the analysis of pairs of elements shows interesting elemental interaction patterns that change from 30 to 45 days of development, suggesting short- or long-term associations, such as storage in similar compartments or relevance for time-dependent biological processes. These findings shed light on which trace elements are important during human brain development and will support studies aimed to unravel the consequences of disrupted metal homeostasis for neurodevelopmental diseases, including those manifested in adulthood.

Introduction

Cerebral development is a lifelong event beginning almost immediately after fertilization. During the third embryonic week, neural tube is formed and before the end of the following week, it compartmentalizes into forebrain, midbrain, and hindbrain. Beginning from the forebrain, the telencephalon evolves towards a complex network with billions of neurons and glial cells in the cerebral cortex, from which organized human thought and behavior will emerge. To a large extent, the blueprint for the postnatal brain is laid out during gestation, when fetal neural cells proliferate, differentiate, migrate, and make connections with other cells. These activities, for the most part, appear to be genetically determined, epigenetically directed, and influenced by the physical and chemical environment of the womb (Georgieff, 2007; Paridaen & Huttner, 2014). Hence, the healthy development of central nervous system (CNS) in the period between the third and seventh week of embryo development is likely to rely on adequate provisions of maternal resources like vitamins or dietary elements.

Nutritional resources available to an embryo in these earliest weeks of life putatively determine some of the most important aspects of future health. One well understood example that relates maternal diet to CNS pathologies is spina bifida, caused by insufficient folic acid in early pregnancy. While less understood, abnormalities in the levels of essential minerals potentially begin *in utero* (Radlowski & Johnson, 2013; Golub & Hogrefe, 2015). Examples of neurological disorders in which micronutrient imbalances have been identified in adulthood include Alzheimer's, Parkinson's, and Huntington's diseases (Miller et al., 2006; Popescu et al., 2009;

Rosas et al., 2012). It is, however, difficult to assess dynamic trace element changes in the developing human brain. Determining expected mineral levels according to developmental stage are of clear importance; however, few studies have successfully addressed this issue. To date, the understanding of mineral inclusion as part of human brain development has only been carried out in post-mortem tissue often involving fixative-treated brains, and inferred from animal models (Wróblewski, Chamberlain & Edström, 1984; Rajan et al., 1997). While analyses on this subject have been conducted on a variety of species, numerous peculiarities including cell types and a distinctive temporal organization make the human brain unique and substantiate the need for in-depth studies of these phenomena in human tissue. One method recently refined to model cellular and molecular events of human embryonic brain development is growing cerebral organoids *in vitro* (Eiraku et al., 2008; Lancaster et al., 2013). These three dimensional structures, derived from human pluripotent stem cells, progressively differentiate and self-organize into physiologically relevant cellular niches that mirror the developing human brain.

In the present work, we used synchrotron radiation based micro X-ray fluorescence (SR-XRF) analysis to detect and quantify trace elements present in human cerebral organoids. We sought to capture the levels and the distribution of minerals in brain tissue during a period of intense cell proliferation versus one in which early neuronal network formation was a dominant developmental feature. This work is the first description of chemical elements composition and distribution in human cerebral organoids.

Materials & Methods

Generation of human induced pluripotent stem cells

Human induced pluripotent stem (iPS) cells were obtained from a skin biopsy as described previously (Sochacki et al., 2016). Briefly, fibroblasts were maintained in culture and then transduced with CytoTune-iPS Sendai reprogramming kit 2.0 (Thermo-Fischer) as per manufacturer's instructions. Then, following colony formation and expansion, cells were checked for pluripotency markers via RT-PCR and ability to differentiate into embryoid bodies (S1 Fig). Skin tissue was obtained after donor signed an informed consent approved by the Research Ethics Committee of Hospital das Clínicas de Porto Alegre (CAPPesq, HCPA, IRB00000921) and by the Research Ethics Committee of Hospital Copa D'Or Rio de Janeiro (CEPCOPADOR, number 727.269).

Human pluripotent stem cells

Human embryonic stem cells (hESC, BR1 cell line) (Fraga et al., 2011) and iPS cells were cultured in mTSeR1 medium (Stemcell Technologies) on Matrigel-coated surface (BD Biosciences). The colonies were manually passaged every seven days and maintained at 37°C in humidified air with 5% CO_2.

Human cerebral organoids

Pluripotent cell differentiation into cerebral organoids was based in a previously described protocol (Lancaster et al., 2013). However, our protocol was conducted mostly using spinner flasks under continuous rotation (Fig 1A). Briefly, human pluripotent stem cells were dissociated with Accutase (Millipore) until obtainment of a single-cell solution. Then, approximately 250,000 cells/mL were inoculated into a spinner flask containing mTeSR1 to final volume of 50 mL, supplemented with 10 μM Y-27632 (Rho-associated protein kinases inhibitor, iRock) (Merck, Millipore) under uninterrupted rotation (40 rpm). After 24h, medium was changed to Dulbecco's modified eagle medium (DMEM)/F12, supplemented with 20% KnockOut™ Serum Replacement (KOSR, Invitrogen), 2 mM Glutamax (Invitrogen), 1% minimum essential medium nonessential amino acids (MEM-NEAA, Gibco), 55 μM 2-Mercaptoethanol (Gibco) and 100 U/mL Penicillin-Streptomycin (Gibco). By day 7, embryoid bodies (EB) were fed with neuroinduction medium composed of DMEM/F12, 1x N2 supplement (Gibco), 2 mM Glutamax (Invitrogen), 1% MEM-NEAA and 1 μg/mL heparin (Sigma) for 4 days. On day 11, cellular aggregates were transferred to petri dishes and embedded in Matrigel for 1h at 37°C and 5% CO_2. Then, cellular aggregates were decanted in a conical tube and returned to a spinner flask containing neurodifferentiation medium composed of 1:1 DMEM/F12: Neurobasal (Gibco), 0.5x N2, 1x B27 minus vitamin A (Gibco), 2 mM Glutamax, 0.5% MEM-NEAA, 0.2 μM 2-Mercaptoethanol and 2.5 μg/mL insulin. After 4 days, cellular aggregates were grown in the aforementioned medium except by replacing with B27 containing vitamin A (Gibco). The medium was changed every week. Cerebral organoids were grown until 30 days of differentiation (totalizing 15 days in neurodifferentiation medium containing vitamin A) and 45 days (totalizing 30 days in neurodifferentiation medium containing vitamin A) for analyses. The

cerebral organoids derived from embryonic stem cells were obtained from two independent assays.

Measurements of cerebral organoid diameter and epithelium-lined cavities total area and number

Cerebral organoids were transferred to non-adherent petri dishes and photographed with an inverted microscope (Eclipse TS100, Nikon). Using ImageJ software (Rasband, W.S., ImageJ, U. S. National Institutes of Health, Bethesda, Maryland, USA, http://imagej.nih.gov/ij/, 1997-2016), cerebral organoid major diameter was measured using the straight-line tool, with reference to the scale bar. The analyzed number of cerebral organoids derived from hESC was as follows: 7-days old organoids, n=107; 15-days old organoids, n=90; 30-days old organoids, n=56; 45-days old organoids, n=18, obtained from two independent experiments. For cerebral organoids derived from iPS cells, the number of cerebral organoids analyzed was as follows: 7-days old organoids, n=8; 15-days old organoids, n=15; 30-days old organoids, n=7; 45-days old organoids, n=10, obtained from one experiment.

To quantify the number of ventricle-like epithelium-lined cavities and to measure their luminal area, tissue sections were stained with hematoxylin and eosin (H&E). Analyzed structures were only considered as ventricle-like cavities when surrounded by a stratified epithelium containing radially organized cells. The number of independent organoids inspected to establish the number of epithelium-lined cavities per organoid was: 30-days old organoids, n=6; 45-days old organoids, n=11. The luminal area was measured with ImageJ software, through delimitation with the freehand selection tool. The number of analyzed ventricles was: 30-days old organoids,

n=17 sections from 6 independent cerebral organoids; 45-days old organoids, n=9 sections from 11 independent cerebral organoids.

Immunohistochemistry

Cerebral organoids were fixed in 4% paraformaldehyde, sequentially incubated in sucrose solutions (10, 20 and 30%) prepared in phosphate buffered saline (PBS), embedded in optimal cutting temperature compound (OCT) and frozen in liquid nitrogen. The organoids were sectioned with a cryostat (Leica) into 20 µm thick sections. Immunofluorescence was performed using the primary antibodies: anti-Nestin (MAB5326, Chemicon), anti-PAX6 (sc11357, Santa Cruz), anti-TBR2 (AB2283, Millipore), anti-class III β-tubulin (T3952, Sigma Aldrich), anti-MAP2 (M1406, Sigma-Aldrich), anti-GAD67 (MAB5406, Chemicon), anti-glutamate (AB133, Chemicon), anti-synaptophysin (MAB368, Chemicon), anti-PSD95 (04-1066, Millipore), and anti-PH3 (06-570, Upstate). Secondary antibodies were used as follows: Alexa Fluor 488 goat anti-mouse (A11001, Invitrogen) and Alexa Fluor 546 goat anti-rabbit (A11010, Invitrogen). DAPI (4', 6-diamidino-2-phenylindole, 1 mg/mL) was used for nuclei staining. Images were acquired using a high content automated microscope (Operetta, Perkin Elmer).

Positive cells for GAD67 and phosphorylated histone 3 (PH3) staining were quantified in the entire section of cerebral organoids. To quantify glutamate intensity, mean gray value (fluorescence intensity) was measured in three points of each cerebral organoid border, delimited by a rectangular selection. The fluorescence intensity in the cerebral organoids' edge was normalized for the tissue background and was given as fold increase in basal condition. The numbers of 30 and 45-days independent samples for quantifications were as follows: PH3

positive cells, n=3 and n=5; MAP2 area, n=4 and n=6; GAD67 positive cells, n=2 and n=4; glutamate fluorescence intensity, n=6 and n=7, respectively.

Synchrotron radiation X-ray fluorescence spectroscopy (SR-XRF) analysis

For XRF analysis, cerebral organoids were quickly rinsed in PBS, embedded in OCT and frozen. Organoids were cut into 30 µm thick sections and placed on ultralene film (transparent to X-ray) and air-dried. Four tissue sections of independent 30-days old cerebral organoids and five sections of independent 45-days old cerebral organoids were analyzed.

The SR-XRF analyses were performed at the D09B X-ray fluorescence beamline at the Brazilian Synchrotron Light Source (Pérez et al., 1999) (Campinas, Brazil) using standard temperature and pressure conditions. Samples were excited by a white beam with energy ranging from 5 keV to 17 keV. An optical system based on a pair of bent mirrors in a Kirkpatrick-Baez arrangement was used to focus the X-ray beam down to 20 µm spatial resolution. Each spot was irradiated for one second. A silicon drift detector (KETEK GmbH) with 140 eV (FWHM) at 5.9 keV placed at 90^{o} from the incident beam was used to collect X-ray fluorescent and scattered radiation coming from samples.

Concentration values in weight fraction units for the elements detected in each pixel of the cerebral organoid slice were determined by the PyMCA software developed by the Software Group of the European Synchrotron Radiation Facility (Solé et al., 2007). After calibrating the spectrometer with a set of pure thin films from Micromatter^{TM} standards (www.micromatter.com), the fundamental parameter method was used (He & Vanespen, 1991). The method predicts the sample matrix effect assuming that the measured primary spectral

204 distribution and excitation-detection geometry are known. The values found in weight fraction
205 units were converted in ppm by multiplying them by a factor 10^6. The mean concentration value
206 was calculated with the values detected in each pixel analyzed per organoid slice.
207

208 Image analyses of trace elements distribution

209 Elemental concentration information was collected from each pixel to generate corresponding
210 XRF maps. The color gradient heat maps were constructed by plotting the fluorescence intensity
211 at each point of the scan using the PyMca software.
212 Images of colored gradient heat maps were converted to grayscale images with Adobe Photoshop
213 CS5 by manually adjusting the hue to match the colors' intensity in RGB images. Then, ImageJ
214 software was used to obtain the intensity profile by drawing a line in sagittal and coronal planes
215 of the organoid images. The generated plot profiles were analyzed in Igor Pro 6 software
216 (Wavemetrics, Lake Oswego, OR, USA) to create curve fittings with polynomial regression of 3
217 terms. The resulting curves were classified as concave or convex. If the fitting result gave rise to
218 a line with less than 10 points of inclination, it was considered as a straight line. We assumed
219 concave as peripheral, convex as central and straight as diffused distribution of the elements
220 within cerebral organoids. Four tissue sections of independent 30-days old cerebral organoids
221 and five sections of independent 45-days old cerebral organoids were analyzed.
222

223 Elemental correlation analysis

224 In order to unveil elements correlation we have used PyMca software to build dot plots
225 combining concentration data for all possible pairs of elements in each scanned pixel. Pearson's
226 correlation coefficient was applied to each element pair, distinguishing correlated and

uncorrelated elements. In addition to Pearson's correlation coefficient, we also fitted a line to each dot plot, generating a R-squared value for each pair of elements. This number was also used as a correlation indicator. A high R-squared above 70% was interpreted as indicator of potentially meaningful associations in paired elements. Finally, color-gradient merged maps were also built using PyMca software, whereas color colocalization indicated elements higher correlation, distinguishable colors were an indicative of unrelated or exclusive elements. Four tissue sections of independent 30-days old cerebral organoids and five sections of independent 45-days old cerebral organoids were analyzed.

Statistical Analyses

Quantitative graphical representations and Table 2 data were reported as mean ± S.D. Analyses of statistical significance were obtained using GraphPad Prism 4 software (GraphPad Software, La Jolla California, USA). Comparisons among organoids' sizes at 7, 15, 30 and 45 days of differentiation were analyzed using one-way ANOVA followed by Tukey's post hoc test.

248

249

250

Results

The growth of human cerebral organoids

253 Exogenous organogenesis using pluripotent stem cells has emerged as a breakthrough
254 technology to study aspects of human brain development in a dynamic and living state
255 (Lancaster et al., 2013). In our preparations, cerebral organoids' differentiation from human
256 embryonic stem cells occurred in spinner flasks as represented in Fig 1A and, by the end of 45
257 days of differentiation, they presented spheroid morphology (Fig 1B). In detail, 30-days old
258 organoids demonstrated different hues and internal folding, suggestive of distinct cell layers
259 (Figs 1C and C'). A period of accelerated growth was observed between the 7^{th} and the 15^{th} day,
260 followed by a period of stationary growth upon retinoic acid addition (15^{th} to 30^{th} day). Then,
261 cerebral organoids continued to expand in size from day 30 to day 45, when they reached 1,240
262 ± 365 μm in diameter (Fig 1D). Cerebral organoids derived from iPS cells also grew in a similar
263 fashion (S2 Fig A-C).
264 As one of our major goals was to generate a cortical anlage from human embryonic stem cells *in*
265 *vitro*, we then examined the cytoarchitecture of the generated cerebral organoids. We focused on
266 two separate time points, 30 and 45 days of differentiation, which corresponded to 15 and 30
267 days, respectively, of exposure to retinoic acid, a crucial morphogen for neuronal induction.
268 Upon 30 days of differentiation, prominent circular structures reminiscent of early ventricles
269 were observed within the organoids (Fig 2A-A'). Interestingly, following organoids' maturation,

the large epithelium-lined cavities were replaced by narrower ones (Fig 2B-B') of reduced luminal area (Fig 2C). Also, the number of putative ventricles or epithelium-lined cavities per cerebral organoid decreased from 30 to 45 days of differentiation (Fig 2D).

Besides substantial differences in size and architecture, we further investigated changes on the expression of neural markers via immunofluorescence. Thirty days into neural differentiation, cells expressing the intermediate filament nestin, characteristic of CNS progenitors, were ubiquitously found in the developing organoids (Fig 3A). Similar to the cortical development *in vivo*, areas immediately adjacent to the ventricle-like cavities had greater cell density and exhibited a radial and outward polarization suggestive of zones of cellular division and migration (Fig 3B). Indeed, the presence of apical progenitors was characterized by mitotic cells lining the luminal surface, positively stained for PH3 (Fig 3B), and by the expression of the transcription factor PAX6 in the putative ventricular zone (Fig 3C). Furthermore, intermediate progenitors expressing the T-box homeobox protein TBR2 were found midway to the putative subventricular zone (SVZ), positioned radially to the luminal surface and adjacent to tangentially migrating neurons (MAP2 positive cells) (Fig 3D) in a cellular architecture similar to the developing cortical plate *in vivo* (Lui, Hansen & Kriegstein, 2011). Likewise, in iPS cells derived cerebral organoids, differentiated neurons were observed positioned in the outer rim of the cellular layer around the putative ventricles, whereas neural progenitors occupied the innermost portion (S2 Fig D-F).

In 45-days old organoids, flattened cavities still presented proliferating cells (PH3 positive cells) and intermediate progenitors (TBR2) in its vicinity, showing their commitment to VZ/SVZ identity (Fig 3E-F). Mature neurons identified by MAP2 staining demonstrated the production of a neuronal primordial plexiform layer organized tangentially to germinal zones (Fig 3G).

Migratory GABAergic neurons were detected by glutamic acid decarboxylase 67 (GAD67) staining in different places in the organoids, primarily near the ventricles (Fig 3H). Concurrently, glutamate was detected in the organoids' edge (Fig 3I). Finally, synaptogenesis was determined by the presence of synaptophysin, a component of presynaptic vesicles, and also by the detection of the postsynaptic density protein 95 (PSD95) (Fig 3J).

As a result of the transitioning from a main self-renewal stage to a neuronal differentiation phase, a 5 times decrease in mitotic activity was observed when comparing the organoids at 30 and 45 days of differentiation (Fig 3K). Accordingly, the amount of mature neurons tripled, as evaluated by MAP2 staining (Fig 3L), and the number of neurons expressing GAD67 increased 4 times (Fig 3M), when comparing organoids at the 30^{th} and at 45^{th} day of differentiation. In addition, peripheral glutamate staining increased 2.5 times (Fig 3N). In line with these data, we considered these two time points (30 and 45 days) to depict two distinct developmental phases: one of pronounced cell division dedicated to tissue expansion and another of early neuronal network formation in cerebral organogenesis. Then, we asked whether these two time points might show different element distribution as they represent two demarcated developmental stages.

SR-XRF microprobe analysis

SR-XRF microprobe was used to scan elements in cerebral organoids. After X-rays excited the sample, each atom emitted a unique, identifiable and quantifiable photon signature. XRF analysis revealed that the major chemical elements in cerebral organoids were phosphorus (P), sulfur (S), potassium (K), calcium (Ca), iron (Fe) and zinc (Zn). The elements manganese (Mn), nickel (Ni) and copper (Cu) were also detected in our preparations, but were not considered further in this study due to their extremely low levels and subsequent classification as ultratrace elements. Although chlorine (Cl) was detected, it was disregarded for further analysis as it was considered

316 a potential laboratorial artifact. While specific roles and importance of the detected elements for
317 brain development or function may be under characterization, some of the known functions are
318 summarized in Table 1.
319

320 Trace elements distribution in human cerebral organoids

321 In order to search for elemental distribution patterns in cerebral organoids, the spectral profile
322 corresponding to each measurable element was collected and assembled into color-gradient heat
323 maps, as represented in Fig 4. Phosphorus could be detected all over organoids' extension,
324 despite being concentrated within the external border in both 30 and 45-days old organoids.
325 Besides being observed diffusely distributed as well, K levels were higher in the organoids' edge
326 in 30 days and then became evenly distributed in 45 days. Sulfur, Ca and Fe displayed a more
327 homogeneous distribution pattern in both proliferative and neuronal differentiation phases.
328 Meanwhile, Zn was mostly diffused in 30-days old organoids and then became peripheral along
329 differentiation process in 45-days old organoids. Elementary pattern distributions revealed a
330 tendency for diffuseness for most elements, with the exceptions of P and Zn. Rather than
331 spreading internally, these two elements continued to be located in higher concentrations in the
332 edge of cerebral organoids.
333

334 Elemental concentration in cerebral organoids

335 To compare the contribution of elements in, here named, proliferative (30 days) and neuronal
336 maturation (45 days) stages, we estimated concentrations of trace elements in parts per million
337 (ppm), which are shown in Fig 5. Phosphorus, S and K were the most abundant elements in both
338 30-days (16,142±1,219 ppm; 4,955±350 ppm and 6,120±1,745 ppm, respectively) and 45-days

339 old organoids (10,286±840 ppm; 4,462±249 ppm and 3,951±422 ppm, respectively). Calcium,
340 Fe and Zn were found in relatively low levels: 192±157 ppm, 84±61 ppm and 129±6 ppm in 30-
341 days old organoids, and 286±43 ppm, 87±37 ppm and 101±2 ppm in 45-days old organoids,
342 respectively. Interestingly, some trace element levels decreased between 30 to 45 days of
343 differentiation, such as P, K and Zn, whereas Fe tended to increase, even though, this latter result
344 did not reach statistical significance.
345 To determine to which degree the presence of trace elements in cerebral organoids could be due
346 to passive diffusion from medium or to active cellular metabolism, we compared elements'
347 availability in cell culture media and in Matrigel with the amounts found within the organoids
348 (S1 and S2 Tables). These quantifications revealed that both cell culture media and Matrigel
349 contributed very poorly to total organoid elemental quantification, being responsible for
350 approximately 0.002% and 0.0000000004% of the amount of trace elements detected in the
351 cerebral organoids, respectively. This substantial disparity strongly suggests that the increased
352 levels of chemical elements observed in cerebral organoids were due to its biological constitution
353 and did not reflect a simple diffusion mechanism.
354

355 Inter-elemental relationship

356 From an initial inspection of the spatial distribution of each element, it was not possible to
357 assess, with any confidence, to which extent they may interact functionally or chemically, as
358 would occur when they become part of biomolecules. We then analyzed elements in pairs to
359 assess coincidental areas, classifying elements as correlated, unrelated or exclusive. Table 2
360 comprises correlation analyses of all possible elemental pairs. We have analyzed elements by
361 Pearson's coefficient correlation and by R-squared values obtained from lines fitted on raw

quantification data. Correlation coefficients closer to 1 indicate higher elemental correlation, while lower correlation coefficients indicate lower elemental correlation. P/S, P/K, P/Zn and S/K were highly correlated elements, as they presented Pearson's correlation coefficients above 0.7 in average. On the other hand, P/Ca, P/Fe, S/Ca, S/Fe, K/Ca, K/Fe, K/Zn, Ca/Zn, Fe/Zn were less correlated pairs of elements, presenting Pearson's correlation coefficients lower than 0.7. Interestingly, the following pairs of elements: P/Ca, S/Ca and K/Ca presented great changes in their correlation coefficients from 30 to 45 days of development (Table 2, 45/30 days ratio), indicating that their behavior might change in a time-dependent manner. Fig 6 comprehends representative color-gradient maps for P/S, P/Zn and K/Ca, highlighting their behavior. Although P/S present a high correlation coefficient, they seem to partly lose colocalization at 45 days (Fig 6A and 6D), which could be seen by elemental distribution within the map. P/Zn (Fig 6B and 6E) presented a similar behavior. Finally, K/Ca (Fig 6C and 6F) presented a very interesting pattern: Ca was particularly localized at 30 days, and evolved to a scattered distribution at 45 days of differentiation.

Discussion

Implications of trace elements detected in cerebral organoids to brain organogenesis

While it is generally accepted that micronutrients are vital to brain morphogenesis, neurochemistry and neurophysiology, well-controlled studies for specific micronutrients are still needed. Furthermore, since most studies on this subject have been done on adult-state or post-mortem tissue samples, little is known about the elemental composition of the developing human CNS. Though it is not an exact replica of a human embryonic brain, exogenously developed cerebral organoids undergo many developmental stages and events that parallel the human condition. Perhaps more importantly, the circuits and structures being constructed contain a significant portion of the human genetic blueprinting and specific neurons that make up the early neuronal networks that give rise to the brain (Lancaster et al., 2013). Therefore, the model used in this study, amongst others of human organogenesis, could be argued to be the closest and most complete study system to date for understanding human neural development and its pathological manifestations.

The methodology for the development of cerebral organoid tissues described in here subtly deviates from the original method reported by Lancaster et al. (2013). Specifically, the aggregation of dissociated pluripotent stem cells into EB was conducted in spinner flasks instead

of using individualized non-adherent 96-well plates. The EB obtained here with iPS cells presented similar sizes when compared to Lancaster's descriptions for those derived from the H9 (WA09) hESC line (Lancaster & Knoblich, 2014). However, EB obtained from the BR1 hESC line were relatively smaller. One possibility is that these results may reflect inter-lineage variability in stem cells aggregation potential, as already described by others (Cahan & Daley, 2013). Importantly, regardless of such difference in EB size, by the end of 30 and 45 days of differentiation, the cytoarchitecture of cerebral organoids' was similar to the original report (Lancaster et al., 2013).

SR-XRF is a suitable technique to scan and image trace elements in brain tissue and has been applied in many models of neurological diseases. The primary advantages in using SR-XRF lie in its low limit of detection, topographic high-resolution chemical imaging and recognition of metal compounds irrespectively of its oxidation state. Given that metal metabolism is disrupted in prevalent neurodegenerative disorders, such as Alzheimer's, Huntington's, and Parkinson's diseases (Popescu et al., 2009; Wang et al., 2012; Muller & Leavitt, 2014), SR-XRF can also be applied for a comprehensive view of metal homeostasis in brain development and aging. Contrary to the research aims carried out by other groups, our study intended to employ SR-XRF on human cerebral organoids to provide us with the first glimpse into which elements may play active roles in early brain development. More specifically, we reported here that P, S, K, Ca, Fe and Zn take part in neural composition during cerebral organoid formation.

Phosphorus was the most heavily represented element. When comparing P levels detected on proliferative (30 days) and neuronal differentiation (45 days) stages, it was significantly decreased. Since P is a structural component of major biomolecules, such as nucleotides and phospholipids, this reduction might be explained by a switch from a phase of intense synthesis,

426 including DNA and phospholipid production, to a more migratory and differentiation phase.
427 With respect to tissue growth, P levels in cerebral organoids were in the same concentration
428 range (mg/g) of that reported for adult brains (Rajan et al., 1997), albeit having been noted here
429 in a higher quantity (Fig 5A). In this regard, the levels found in our study imply a greater
430 participation of P during the development of neural tissue (Rajan et al., 1997). Silvestre and
431 colleagues (2009) also showed that total lipid P content is higher in the embryonic brain than in
432 adult brain cells (Silvestre, Maccioni & Caputto, 2009). The developing brain contains superior
433 concentrations of phosphate groups belonging to lecithins, cephalins, and sphingomyelins, this
434 could explain the different values found in our study. This dissimilarity underscores the need for
435 pursuing elemental changes at either end of the aging spectrum.
436 Cerebral organoids were also shown to contain significant levels of K and S. Potassium is
437 essential to transmembrane transport, regulation of cellular volume, and membrane resting
438 potential. During brain ontogenesis, K regulates proliferation of neural progenitors (Achilles et
439 al., 2007; Yasuda, Bartlett & Adams, 2008; Schaarschmidt et al., 2009) and is maintained in
440 heightened levels in rapidly dividing cells (Cameron, Pool & Smith, 1979; Wallberg et al.,
441 2000). As K currents also support the migration of early neurons over long distances due to
442 cellular volume changes (Hendriks, Morest & Kaczmarek, 1999), we can speculate from our data
443 that it could be important to maintain mitotic activity in 30-days old organoids and to promote
444 cell migration in 45-days old organoids, amongst other roles.
445 It is known that S integrates virtually all proteins through methionine and cysteine amino acids
446 and disulfide bounds. In the embryonic cerebrum, chondroitin and heparan sulfate proteoglycans
447 anchor attractive and/or repulsive cues such as growth factors, chemokines, axon guidance
448 molecules, and cell adhesion molecules important for neuronal migration in strategically routes

449 such as the striatum, marginal zone, subplate, and subventricular zone in the neocortex (Maeda,
450 2015). As an example, brains devoid of perlecan, a heparan sulfate proteoglycan component of
451 the CNS extracellular matrix, have impaired cortical development and are microcephalic (Girós
452 et al., 2007). Beyond this, S is also incorporated in proteoglycans expressed in the basal lamina
453 of the neuroepithelium that regulates neurogenesis in the developing telencephalon (Girós et al.,
454 2007). In cerebral organoids, we found high levels of S, both in 30 and 45 days of differentiation,
455 pointing to its central role in organoids' patterning. Therefore, we postulate that S may play a
456 fundamental role in brain construction and in organoids' scaffolding and patterning.
457 The metallic elements Ca, Fe, and Zn, which are essential for brain morphogenesis, were found
458 in the μg/g range in cerebral organoids. Calcium participates in a variety of cellular functions in
459 different areas extending from proliferative zones to post mitotic intermediate zone and marginal
460 zone. In neural progenitor cells, Ca waves, sustained by IP3-signaling, control cell proliferation
461 (Weissman et al., 2004; Resende et al., 2010), while Ca influx via ion channels influences cell
462 differentiation (Shin et al., 2010). Importantly, during early neurogenesis, the expression of
463 transcription factors regulating neuronal survival and differentiation can be controlled by Ca
464 (Leclerc et al., 2012). Noteworthy, Ca ppm values detected in the present work are consistent
465 with those found by Riederer et al. (1989) and Rajan et al. (1997) in human cerebrum cortex
466 (Riederer et al., 1989; Rajan et al., 1997) (Fig 5D and S3 Table). Altogether, these findings
467 emphasize that Ca may pave the way to brain organogenesis.
468 Zinc is an essential element to protein synthesis, enzymatic catalysis and serves as a structural
469 component to zinc finger transcription factors. Zinc dependent enzymes include
470 metalloproteinases and many intermediary metabolism dehydrogenases important for CNS
471 function (Tapiero & Tew, 2003). In addition, chelatable Zn present in synaptic vesicles can be

472 released in the synaptic cleft to modulate many synaptic activities (Marger, Schubert & Bertrand,
473 2014). In comparison to previous studies in adult brain, we found higher levels of Zn in cerebral
474 organoids (Katoh, Sato & Yamamoto, 2002; Rahil-Khazen et al., 2002), although compatible in
475 scale of dosage (Fig 5F). While greater concentrations of Zn in adult brain are toxic to neural
476 cells and also cause axonal degeneration in mice (Chuah, Tennent & Jacobs, 1995), Zn
477 modulates stem cell proliferation and neuronal differentiation during neurogenesis (Gao et al.,
478 2009; Levenson & Morris, 2011; Morris & Levenson, 2013). In accordance, previous data from
479 our group have demonstrated increased Zn during neural differentiation of human pluripotent
480 stem cells (Cardoso et al., 2011). This may highlight the importance of Zn for neural stem cells
481 commitment and justify why the levels found in cerebral organoids are subtly higher than those
482 described in adult brain (Fig 3F and S3 Table) (Dexter et al., 1991; Rajan et al., 1997; Rahil-
483 Khazen et al., 2002).
484 It is currently known that Fe accumulates during brain prenatal development, with the highest
485 levels observed immediately after birth. In the developing brain, Fe is required in rapidly
486 developing regions such as the cerebral cortex (Siddappa et al., 2003) in heme-containing
487 cytochromes that regulate neuronal and glial energetic status (Evans & Mackler, 1985). Along
488 the same line, Fe is required to the initial expansion of neural tissue and by neurogenesis, which
489 may account for its levels in the present study. It is noteworthy that the Fe values found for
490 cerebral organoids parallel those measured in the adult brain (Sofic et al., 1988; Dexter et al.,
491 1991; Rajan et al., 1997; Rahil-Khazen et al., 2002). Although higher Fe concentrations are
492 found in some specific cerebral regions such as substantia nigra, putamen and globus pallidus
493 (Dexter et al., 1991), they were not represented in this study. As examples of Fe roles in the
494 CNS, Fe-containing enzymes are essential for tyrosine and tryptophan hydroxylase activities and

for monoamine catabolism in synapses. Besides, Fe is also required for ribonucleotide reductase in order to regulate cell division and for normal myelination throughout CNS development (Lozoff & Georgieff, 2006).

Overall, cerebral organoids derived from pluripotent stem cells presented an elemental composition mostly compatible with previous reports (Fig 5 and S3 Table). However, some discrepancies can be found, such as Fe levels. We have found approximately 90 ppm, while values reported for fresh harvested autopsies are still diverging, including 225 ppm in cerebral cortex in the motor field (Katoh, Sato & Yamamoto, 2002), 101 ppm in the precentral gyrus (Popescu and Nichol, 2011), and 50.2 ppm in the brain front lobe (Rahil-Khazen et al., 2002). Considering that these studies were performed on adult tissue samples, while cerebral organoids generated *in vitro* are an embryonic model, these differences can be attributed to sample origin. Another possibility is that *in vivo* models surpass elemental concentrations observed in *in vitro* models, as already reported for murine cultured neurons and astrocytes (Hare et al., 2013). Nevertheless, we believe that proper organoid quantifications are relevant, especially when comparing healthy vs. pathological conditions, such as in our work on iPS cells derived from schizophrenic patient (Paulsen et al., 2014).

Analysis of different organs also revealed similarities and differences from neural tissues and our cerebral organoids. Reports on Fe content in breast (~5 ppm) (Geraki, Farquharson & Bradley, 2002), heart (257 ppm), kidney (430 ppm), liver (837 ppm), lungs (987 ppm) (Katoh, Sato & Yamamoto, 2002), among other organs, reveal actual variation intervals (5 to 987 ppm). With 3D organoid technology boosting *in vitro* human organs modeling, we believe that elemental characterization will be a relevant tool for assessing general and discrete processes within these

models, in addition to revealing chemical patterns and enabling *in vivo* vs. *in vitro* and/or healthy vs. pathologic state comparisons.

Trace elements distribution in human cerebral organoids

Our data indicate that trace elements change their distribution inside organoids along differentiation. It is known that some molecules can pass through cell membrane by simple diffusion or with the aid of specific cellular transporters or channels. Potassium was reported as firstly concentrated at the organoids' border and then became evenly distributed inside. Since K is positively charged and therefore not permeant to cell membranes, one possibility is that NKCC1, an inwardly directed cotransporter, begins to be expressed and might contribute to the simultaneous K and Cl influx. NKCC1 expression is upregulated in early developmental stages and downregulated in later brain development *in vivo* (Kaila et al., 2014).

Even though the distribution profile of a given element may be associated with changes in the expression of specific receptors and/or channels in the organoid, one can also suggest a particular role for such element in a specific cellular niche. For example, Zn displayed a more homogeneous distribution within organoids, but became relatively more peripheral at 45 days. Of note, glutamate was almost undetectable in organoids at 30 days of differentiation, but at 45 days, it occupied the outer portion of the organoids. It is known that Zn is present at high levels in glutamatergic synaptic vesicles of forebrain neurons and that its influx can be mediated by AMPA channels (Martínez-Galán, Díaz & Juiz, 2003; Takeda et al., 2009). Beyond this, Zn-dependent metalloproteinases facilitate neural migration and regulate neurite outgrowth in the preplate and cortical plate (Sanz, Ferraro & Fournier, 2015; Sîrbulescu, Ilieş & Zupanc, 2015). Hence, one possibility is that Zn intensity matches cellular distribution of glutamatergic cells and

neuronal synaptogenesis. In this regard, further studies should help identify changes in the expression of specific channels and receptors that may take part in microelemental homeostasis of cerebral organoids.

There is another very important feature that has to be taken into account when discussing element distribution in cerebral organoids: cell density. Both organoid groups, 30 and 45 days of differentiation, presented increased cell density in organoids' edge. In 30-days old organoids, edges had 3.9 times more cells than the center, while in 45-days old organoids this difference decreased to 1.3 times (data not shown). This behavior may explain the fact that K was mainly present near the edge in 30-days old organoids and became more diffuse in 45-days old organoids. Nevertheless, cell density did not influence S, Ca, and Fe distribution, as these elements do not followed K pattern. Also, Zn was only concentrated near the edge at 45 days of development.

Inter-elemental correlations in human cerebral organoids

The atomic elements can exist freely intra and extracellularly in the form of ions or ionic groups, and in association with biomolecules, for example. These associations define or, are defined by cellular processes, in which two or more elements behave in similar ways. Associations of this kind can be investigated by elemental correlation studies. Our analysis revealed interesting patterns, as P, S, K and Zn seem to be highly correlated, whereas Ca and Fe present very low correlation levels. In addition, we also found that P, S, Zn, K and Ca change their correlation pattern from 30 to 45 days of differentiation. These phenomena are interesting as they may portrait the change from a proliferation to a neuronal maturation stage during organoid development.

Zinc is not only a structural element, but also acts as a regulator of cell proliferation. Based on studies with Zn chelators in mammalian cells, it was found that Zn deficiency results in reduced expression of thymidine kinase (Chesters, Petrie & Travis, 1990) and reduction in thymidine incorporation (Chesters, Petrie & Vint, 1989). Strictly, Zn integrates DNA polymerase (Springgate et al., 1973), RNA polymerase (Wu et al., 1992), and ribosomal proteins (Härd et al., 2000). Whilst purely speculative, it is possible that P, as being part of nucleic acids and present in proteins, shares the same location with Zn, as both are involved in cell proliferation and protein synthesis. Another interesting example is K, which seems to be directly involved in the control of protein synthesis (Lubin & Ennis, 1964) and, in conjunction with P, is enriched in ribosomes. Specifically in neurons, K tends to correlate with P in the adult rat brain (Cameron, Sheridan & Smith, 1978). In a previous work from our group, we have shown that neurospheres generated from iPS cells derived from schizophrenia patient biopsies present higher levels of Zn and K, while producing high levels of reactive oxygen species (ROS) (Paulsen et al, 2013). Despite the fact that these studies did not involve direct correlation between metals and biomolecules, we were able to link this correlation to a disease model involving Zn defective transport leading to K imbalance. In sum, we conclude that element correlation is a fundamental part of SR-XRF analysis, especially taking into consideration the organoid model, since its cellular organization is much more complex than EB and neurospheres.

Functional significance

Mounting evidence indicates that maternal malnutrition may be causative in many neurocognitive deficits and neurological diseases in offspring (Felt & Lozoff, 1996; de Souza, Fernandes & do Carmo, 2011). Given that maternal diet is the principle source of dietary

586 elements available to a developing fetus; our data highlight the importance of matching the
587 essential elements P, S, K, Ca, Fe and Zn to developmental needs of the brain. For instance,
588 deficiencies in Zn nutrition during prenatal development are associated with offspring learning
589 and memory paucity (Liu et al., 1992; Tahmasebi Boroujeni et al., 2009; Yu et al., 2013), in part
590 caused by decreased expression of brain-derived neurotrophic factor (BDNF), altered myelin
591 composition (Liu et al., 1992) and declined long-term potentiation (Yu, Ren & Yu, 2013).
592 Gestational Fe anemia, the most common nutritional need, can impact learning, memory, and
593 motor abilities in progeny. These poor executive performances can be explained at the cellular
594 level by decreased synaptic maturity, dopamine metabolism and myelin composition (Lozoff &
595 Georgieff, 2006). In a prospective study, it was found that maternal Fe deficiency may be a risk
596 for schizophrenia in offspring (Insel et al., 2008). This means that mother's diet during
597 pregnancy can have long-term consequences in fetal brain structuring.

598

599 Conclusions

600 Here, we have shown the potential of cerebral organoids in conjunction to XRF analysis to
601 explore minerals homeostasis during brain development. Mapping each micronutrient could be
602 useful for indicating the expression of specific receptors and/or channels, as well as for locating
603 elements that take part in neural composition during cerebral organogenesis, such as P, S, K, Ca,
604 Fe and Zn in a particular cellular niche. Also, mathematical analyses such as Pearson's
605 correlation coefficients and R-squared values for pairs of elements could give a glimpse of
606 chemical or functional interactions.

607 Trace element levels in normal and pathological brain development are central to establish cause
608 and effect relationships, mainly for nutritional deficiencies or metal transporter inabilities and
609 other disorders in which trace elements are involved. Nowadays, many diseases have been
610 regarded as neurodevelopmental disorders, with its roots planted in the first months or years of
611 life. Disturbances in early brain development have been deemed important for later developing
612 Parkinson's disease or schizophrenia (Piper et al., 2012; Le Grand et al., 2015). Therefore, it
613 seems reasonable to emphasize the need to gather data on normal trace element levels in
614 embryonic brain tissue as presented in this work. In conclusion, cerebral organoids derived from
615 pluripotent stem cells recapitulate features of trace element constitution previously described in
616 the human brain.
617
618
619
620

621 # Acknowledgments

622 We are indebted to Ismael Gomes, Gabriela Lopes Vitória, Marcelo Costa and Jarek Sochacki
623 for taking excellent care of cell lines.
624

References

Achilles K, Okabe A, Ikeda M, Shimizu-Okabe C, Yamada J, Fukuda A, Luhmann HJ, Kilb W. 2007. Kinetic properties of Cl uptake mediated by Na+-dependent K+-2Cl cotransport in immature rat neocortical neurons. *The Journal of neuroscience : the official journal of the Society for Neuroscience* 27:8616–8627. DOI: 10.1523/JNEUROSCI.5041-06.2007.

Atlas D. 2013. The voltage-gated calcium channel functions as the molecular switch of synaptic transmission. *Annual review of biochemistry* 82:607–35. DOI: 10.1146/annurev-biochem-080411-121438.

Cahan P, Daley GQ. 2013. Origins and implications of pluripotent stem cell variability and heterogeneity. *Nature reviews. Molecular cell biology* 14:357–68. DOI: 10.1038/nrm3584.

Cameron IL, Pool TB, Smith NK. 1979. An X-ray microanalysis survey of the concentration of elements in the cytoplasm of different mammalian cell types. *Journal of cellular physiology* 101:493–501. DOI: 10.1002/jcp.1041010315.

Cameron IL, Sheridan PJ, Smith NR. 1978. An x-ray microanalysis study of differences in concentration of elements in brain cells due to opiates, cell type, and subcellular location. *Journal of neuroscience research* 3:397–410.

Cardoso SC, Stelling MP, Paulsen BS, Rehen SK. 2011. Synchrotron radiation X-ray microfluorescence reveals polarized distribution of atomic elements during differentiation of pluripotent stem cells. *PLoS ONE* 6:1–10. DOI: 10.1371/journal.pone.0029244.

Chesters JK, Petrie L, Travis AJ. 1990. A requirement for Zn2+ for the induction of thymidine kinase but not ornithine decarboxylase in 3T3 cells stimulated from quiescence. *The Biochemical journal* 272:525–7.

Chesters JK, Petrie L, Vint H. 1989. Specificity and timing of the Zn2+ requirement for DNA synthesis by 3T3 cells. *Experimental cell research* 184:499–508.

Chuah MI, Tennent R, Jacobs I. 1995. Response of olfactory Schwann cells to intranasal zinc sulfate irrigation. *Journal of neuroscience research* 42:470–8. DOI: 10.1002/jnr.490420405.

Dexter DT, Carayon A, Javoy-Agid F, Agid Y, Wells FR, Daniel SE, Lees AJ, Jenner P, Marsden CD. 1991. Alterations in the levels of iron, ferritin and other trace metals in Parkinson's disease and other neurodegenerative diseases affecting the basal ganglia. *Brain : a journal of neurology* 114 (Pt 4:1953–75.

Eiraku M, Watanabe K, Matsuo-Takasaki M, Kawada M, Yonemura S, Matsumura M, Wataya T, Nishiyama A, Muguruma K, Sasai Y. 2008. Self-organized formation of polarized cortical tissues from ESCs and its active manipulation by extrinsic signals. *Cell stem cell* 3:519–32. DOI: 10.1016/j.stem.2008.09.002.

Erikson KM, Jones BC, Hess EJ, Zhang Q, Beard JL. 2001. Iron deficiency decreases dopamine D1 and D2 receptors in rat brain. *Pharmacology, biochemistry, and behavior* 69:409–18.

Evans TC, Mackler B. 1985. Effect of iron deficiency on energy conservation in rat liver and skeletal muscle submitochondrial particles. *Biochemical medicine* 34:93–9.

665 Felt BT, Lozoff B. 1996. Brain iron and behavior of rats are not normalized by treatment of iron
666 deficiency anemia during early development. *The Journal of nutrition* 126:693–701.

667 Fraga AM, Sukoyan M, Rajan P, Braga DP de AF, Iaconelli A, Franco JG, Borges E, Pereira L
668 V. 2011. Establishment of a Brazilian line of human embryonic stem cells in defined
669 medium: implications for cell therapy in an ethnically diverse population. *Cell*
670 *transplantation* 20:431–40. DOI: 10.3727/096368910X522261.

671 Gao H-L, Zheng W, Xin N, Chi Z-H, Wang Z-Y, Chen J, Wang Z-Y. 2009. Zinc deficiency
672 reduces neurogenesis accompanied by neuronal apoptosis through caspase-dependent and -
673 independent signaling pathways. *Neurotoxicity research* 16:416–25. DOI: 10.1007/s12640-
674 009-9072-7.

675 Georgieff MK. 2007. Nutrition and the developing brain: nutrient priorities and measurement.
676 *The American journal of clinical nutrition* 85:614S–620S.

677 Geraki K., Farquharson MJ., Bradley D a. 2002. Concentrations of Fe, Cu and Zn in breast
678 tissue: a synchrotron XRF study. *Physics in medicine and biology* 47:2327–2339. DOI:
679 10.1088/0031-9155/47/13/310.

680 Girós A, Morante J, Gil-Sanz C, Fairén A, Costell M. 2007. Perlecan controls neurogenesis in
681 the developing telencephalon. *BMC developmental biology* 7:29. DOI: 10.1186/1471-213X-
682 7-29.

683 Golub MS, Hogrefe CE. 2015. Fetal iron deficiency and genotype influence emotionality in
684 infant rhesus monkeys. *The Journal of nutrition* 145:647–53. DOI: 10.3945/jn.114.201798.

685 Le Grand JN, Gonzalez-Cano L, Pavlou MA, Schwamborn JC. 2015. Neural stem cells in
686 Parkinson's disease: a role for neurogenesis defects in onset and progression. *Cellular and*
687 *molecular life sciences : CMLS* 72:773–97. DOI: 10.1007/s00018-014-1774-1.

688 Härd T, Rak A, Allard P, Kloo L, Garber M. 2000. The solution structure of ribosomal protein
689 L36 from Thermus thermophilus reveals a zinc-ribbon-like fold. *Journal of molecular*
690 *biology* 296:169–80. DOI: 10.1006/jmbi.1999.3433.

691 Hare DJ., Grubman A., Ryan TM., Lothian A., Liddell JR., Grimm R., Matsuda T., Doble PA.,
692 Cherny RA., Bush AI., White AR., Masters CL., Roberts BR. 2013. Profiling the iron,
693 copper and zinc content in primary neuron and astrocyte cultures by rapid online
694 quantitative size exclusion chromatography- inductively coupled plasma-mass
695 spectrometry. *Metallomics* 5:1656–1662. DOI: 10.1039/c3mt00227f.

696 He F., Vanespen pj. 1991. General-approach for quantitative energy dispersive-x-ray
697 fluorescence analysis based on fundamental parameters. *Analytical Chemistry* 63:2237–
698 2244.

699 Hendriks R, Morest DK, Kaczmarek LK. 1999. Role in neuronal cell migration for high-
700 threshold potassium currents in the chicken hindbrain. *Journal of neuroscience research*
701 58:805–14.

702 Inatani M, Irie F, Plump AS, Tessier-Lavigne M, Yamaguchi Y. 2003. Mammalian brain
703 morphogenesis and midline axon guidance require heparan sulfate. *Science (New York,*
704 *N.Y.)* 302:1044–1046. DOI: 10.1126/science.1090497.

Insel BJ, Schaefer C a, McKeague IW, Susser ES, Brown AS. 2008. Maternal iron deficiency and the risk of schizophrenia in offspring. *Archives of general psychiatry* 65:1136–1144. DOI: 10.1001/archpsyc.65.10.1136.

Kaila K, Price TJ, Payne J a, Puskarjov M, Voipio J. 2014. Cation-chloride cotransporters in neuronal development, plasticity and disease. *Nature Publishing Group* 15:637–654. DOI: 10.1038/nrn3819.

Katoh Y., Sato T., Yamamoto Y. 2002. Determination of multielement concentrations in normal human organs from the Japanese. *Biological trace element research* 90:57–70. DOI: 10.1385/BTER:90:1-3:57.

Lancaster MA, Renner M, Martin C-A, Wenzel D, Bicknell LS, Hurles ME, Homfray T, Penninger JM, Jackson AP, Knoblich JA. 2013. Cerebral organoids model human brain development and microcephaly. *Nature* 501:373–9. DOI: 10.1038/nature12517.

Lancaster MA, Knoblich JA. 2014. Generation of cerebral organoids from human pluripotent stem cells. *Nature protocols* 9:2329–2340. DOI: 10.1038/nprot.2014.158.

Leclerc C, Néant I, Moreau M, Hansen D V, Lui JH, Parker PRL, Kriegstein AR. 2012. The calcium: an early signal that initiates the formation of the nervous system during embryogenesis. *Frontiers in Molecular Neuroscience* 5:1–12. DOI: 10.3389/fnmol.2012.00064.

Levenson CW, Morris D. 2011. Zinc and Neurogenesis: Making New Neurons from Development to Adulthood. *Advances in Nutrition: An International Review Journal* 2:96–100. DOI: 10.3945/an.110.000174.

Liu H, Oteiza PI, Gershwin ME, Golub MS, Keen CL. 1992. Effects of maternal marginal zinc deficiency on myelin protein profiles in the suckling rat and infant rhesus monkey. *Biological trace element research* 34:55–66. DOI: 10.1007/BF02783898.

Lozoff B, Georgieff MK. 2006. Iron Deficiency and Brain Development. *Seminars in Pediatric Neurology* 13:158–165. DOI: 10.1016/j.spen.2006.08.004.

Lubin M, Ennis HL. 1964. on the Role of Intracellular Potassium in Protein Synthesis. *Biochimica et biophysica acta* 80:614–631. DOI: 10.1016/0926-6550(64)90306-8.

Lui JH, Hansen D V., Kriegstein AR. 2011. Development and evolution of the human neocortex. *Cell* 146:18–36. DOI: 10.1016/j.cell.2011.06.030.

Maeda N. 2015. Proteoglycans and neuronal migration in the cerebral cortex during development and disease. *Frontiers in Neuroscience* 9:1–15. DOI: 10.3389/fnins.2015.00098.

Marger L, Schubert CR, Bertrand D. 2014. Zinc: an underappreciated modulatory factor of brain function. *Biochemical pharmacology* 91:426–35. DOI: 10.1016/j.bcp.2014.08.002.

Martínez-Galán JR, Díaz C, Juiz JM. 2003. Histochemical localization of neurons with zinc-permeable AMPA/kainate channels in rat brain slices. *Brain research* 963:156–64.

Miller LM, Wang Q, Telivala TP, Smith RJ, Lanzirotti A, Miklossy J. 2006. Synchrotron-based infrared and X-ray imaging shows focalized accumulation of Cu and Zn co-localized with β-amyloid deposits in Alzheimer's disease. *Journal of Structural Biology* 155:30–37. DOI: 10.1016/j.jsb.2005.09.004.

Morris DR, Levenson CW. 2013. Zinc regulation of transcriptional activity during retinoic acid-induced neuronal differentiation. *Journal of Nutritional Biochemistry* 24:1940–1944. DOI: 10.1016/j.jnutbio.2013.06.002.

Muller M, Leavitt BR. 2014. Iron dysregulation in Huntington's disease. *Journal of neurochemistry* 130:328–50. DOI: 10.1111/jnc.12739.

Paridaen JTML, Huttner WB. 2014. Neurogenesis during development of the vertebrate central nervous system. *EMBO reports* 15:351–64. DOI: 10.1002/embr.201438447.

Paulsen B da S., Cardoso SC., Stelling MP., Cadilhe DV., Rehen SK. 2014. Valproate reverts zinc and potassium imbalance in schizophrenia-derived reprogrammed cells. *Schizophrenia research* 154:30–5. DOI: 10.1016/j.schres.2014.02.007.

Pérez CA, Radtke M, Sánchez HJ, Tolentino H, Neuenshwander RT, Barg W, Rubio M, Bueno MIS, Raimundo IM, Rohwedder JJR. 1999. Synchrotron radiation X-Ray fluorescence at the LNLS: beamline instrumentation and experiments. *X-Ray Spectrometry* 28:320–326. DOI: 10.1002/(SICI)1097-4539(199909/10)28:5<320::AID-XRS359>3.0.CO;2-1.

Piper M, Beneyto M, Burne THJ, Eyles DW, Lewis D a., McGrath JJ. 2012. The Neurodevelopmental Hypothesis of Schizophrenia. Convergent Clues from Epidemiology and Neuropathology. *Psychiatric Clinics of North America* 35:571–584. DOI: 10.1016/j.psc.2012.06.002.

Popescu BFG, George MJ, Bergmann U, Garachtchenko A V, Kelly ME, McCrea RPE, Lüning K, Devon RM, George GN, Hanson AD, Harder SM, Chapman LD, Pickering IJ, Nichol H. 2009. Mapping metals in Parkinson's and normal brain using rapid-scanning x-ray fluorescence. *Physics in medicine and biology* 54:651–663. DOI: 10.1088/0031-9155/54/3/012.

Radlowski EC, Johnson RW. 2013. Perinatal iron deficiency and neurocognitive development. *Frontiers in human neuroscience* 7:585. DOI: 10.3389/fnhum.2013.00585.

Rahil-Khazen R, Bolann BJ, Myking A, Ulvik RJ. 2002. Multi-element analysis of trace element levels in human autopsy tissues by using inductively coupled atomic emission spectrometry technique (ICP-AES). *Journal of trace elements in medicine and biology : organ of the Society for Minerals and Trace Elements (GMS)* 16:15–25. DOI: 10.1016/S0946-672X(02)80004-9.

Rajan MT, Jagannatha Rao KS, Mamatha BM, Rao R V, Shanmugavelu P, Menon RB, Pavithran M V. 1997. Quantification of trace elements in normal human brain by inductively coupled plasma atomic emission spectrometry. *Journal of the neurological sciences* 146:153–66.

Resende RR, Adhikari A, da Costa JL, Lorençon E, Ladeira MS, Guatimosim S, Kihara AH, Ladeira LO. 2010. Influence of spontaneous calcium events on cell-cycle progression in embryonal carcinoma and adult stem cells. *Biochimica et biophysica acta* 1803:246–60. DOI: 10.1016/j.bbamcr.2009.11.008.

Riederer P, Sofic E, Rausch WD, Schmidt B, Reynolds GP, Jellinger K, Youdim MB. 1989. Transition metals, ferritin, glutathione, and ascorbic acid in parkinsonian brains. *Journal of neurochemistry* 52:515–20.

785 Rosas HD, Chen YI, Doros G, Salat DH, Chen N, Kwong KK, Bush A, Fox J, Hersch SM. 2012.
786 Alterations in brain transition metals in Huntington disease: an evolving and intricate story.
787 *Archives of neurology* 69:887–93. DOI: 10.1001/archneurol.2011.2945.

788 Sanz R, Ferraro GB, Fournier AE. 2015. IgLON cell adhesion molecules are shed from the cell
789 surface of cortical neurons to promote neuronal growth. *The Journal of biological chemistry*
790 290:4330–42. DOI: 10.1074/jbc.M114.628438.

791 Schaarschmidt G, Wegner F, Schwarz SC, Schmidt H, Schwarz J. 2009. Characterization of
792 voltage-gated potassium channels in human neural progenitor cells. *PLoS ONE* 4. DOI:
793 10.1371/journal.pone.0006168.

794 Shin HY, Hong YH, Jang SS, Chae HG, Paek SL, Moon HE, Kim DG, Kim J, Paek SH, Kim SJ.
795 2010. A role of canonical transient receptor potential 5 channel in neuronal differentiation
796 from A2B5 neural progenitor cells. *PloS one* 5:e10359. DOI:
797 10.1371/journal.pone.0010359.

798 Siddappa AJM, Rao RB, Wobken JD, Casperson K, Leibold EA, Connor JR, Georgieff MK.
799 2003. Iron deficiency alters iron regulatory protein and iron transport protein expression in
800 the perinatal rat brain. *Pediatric research* 53:800–7. DOI:
801 10.1203/01.PDR.0000058922.67035.D5.

802 Silvestre DC, Maccioni HJF, Caputto BL. 2009. Content of endoplasmic reticulum and golgi
803 complex membranes positively correlates with the proliferative status of brain cells. *Journal*
804 *of Neuroscience Research* 87:857–865. DOI: 10.1002/jnr.21915.

805 Sîrbulescu RF, Ilieş I, Zupanc GKH. 2015. Matrix metalloproteinase-2 and -9 in the cerebellum
806 of teleost fish: Functional implications for adult neurogenesis. *Molecular and cellular*
807 *neurosciences* 68:9–23. DOI: 10.1016/j.mcn.2015.03.015.

808 Sochacki J, Devalle S, Reis M, Mattos P, Rehen S. 2016. Generation of iPS cell lines from
809 schizophrenia patients using a non-integrative method. *Stem Cell Research*. DOI:
810 10.1016/j.scr.2016.05.015.

811 Sofic E, Riederer P, Heinsen H, Beckmann H, Reynolds GP, Hebenstreit G, Youdim MB. 1988.
812 Increased iron (III) and total iron content in post mortem substantia nigra of parkinsonian
813 brain. *Journal of neural transmission* 74:199–205.

814 Solé VA., Papillon E., Cotte M., Walter P., Susini J. 2007. A multiplatform code for the analysis
815 of energy-dispersive X-ray fluorescence spectra. *Spectrochimica Acta - Part B Atomic*
816 *Spectroscopy* 62:63–68. DOI: 10.1016/j.sab.2006.12.002.

817 De Souza AS, Fernandes FS, do Carmo M das GT. 2011. Effects of maternal malnutrition and
818 postnatal nutritional rehabilitation on brain fatty acids, learning, and memory. *Nutrition*
819 *reviews* 69:132–44. DOI: 10.1111/j.1753-4887.2011.00374.x.

820 Springgate CF, Mildvan AS, Abramson R, Engle JL, Loeb LA. 1973. Escherichia coli
821 deoxyribonucleic acid polymerase I, a zinc metalloenzyme. Nuclear quadrupolar relaxation
822 studies of the role of bound zinc. *The Journal of biological chemistry* 248:5987–93.

823 Tahmasebi Boroujeni S, Naghdi N, Shahbazi M, Farrokhi A, Bagherzadeh F, Kazemnejad A,
824 Javadian M. 2009. The effect of severe zinc deficiency and zinc supplement on spatial
825 learning and memory. *Biological trace element research* 130:48–61. DOI: 10.1007/s12011-
826 008-8312-7.

827 Takeda A, Sakurada N, Ando M, Kanno S, Oku N. 2009. Facilitation of zinc influx via
828 AMPA/kainate receptor activation in the hippocampus. *Neurochemistry international*
829 55:376–82. DOI: 10.1016/j.neuint.2009.04.006.

830 Tapiero H, Tew KD. 2003. Trace elements in human physiology and pathology: zinc and
831 metallothioneins. *Biomedicine & pharmacotherapy = Biomédecine & pharmacothérapie*
832 57:399–411.

833 Tran P V, Carlson ES, Fretham SJB, Georgieff MK. 2008. Early-life iron deficiency anemia
834 alters neurotrophic factor expression and hippocampal neuron differentiation in male rats.
835 *The Journal of nutrition* 138:2495–501. DOI: 10.3945/jn.108.091553.

836 VanLandingham JW, Levenson CW. 2003. Effect of retinoic acid on ferritin H expression during
837 brain development and neuronal differentiation. *Nutritional neuroscience* 6:39–45. DOI:
838 10.1080/1028415021000056041.

839 Wallberg P, Lindberg M, Alsterborg E, Roomans GM, Wróblewski R. 2000. Elemental changes
840 in skin from patients with basal cell carcinoma. *Journal of submicroscopic cytology and*
841 *pathology* 32:169–73.

842 Wang H, Wang M, Wang B, Li M, Chen H, Yu X, Yang K, Chai Z, Zhao Y, Feng W. 2012.
843 Immunogold labeling and X-ray fluorescence microscopy reveal enrichment ratios of Cu
844 and Zn, metabolism of APP and amyloid-β plaque formation in a mouse model of
845 Alzheimer's disease. *Metallomics : integrated biometal science* 4:1113–8. DOI:
846 10.1039/c2mt20056b.

847 Weissman TA, Riquelme PA, Ivic L, Flint AC, Kriegstein AR. 2004. Calcium waves propagate
848 through radial glial cells and modulate proliferation in the developing neocortex. *Neuron*
849 43:647–61. DOI: 10.1016/j.neuron.2004.08.015.

850 Wróblewski R, Chamberlain J, Edström L. 1984. Sodium, phosphorus, sulphur, chlorine and
851 potassium shifts in rat brain during embryonic development. *Brain research* 314:207–15.

852 Wu FY, Huang WJ, Sinclair RB, Powers L. 1992. The structure of the zinc sites of Escherichia
853 coli DNA-dependent RNA polymerase. *The Journal of biological chemistry* 267:25560–7.

854 Yasuda T, Bartlett PF, Adams DJ. 2008. K(ir) and K(v) channels regulate electrical properties
855 and proliferation of adult neural precursor cells. *Molecular and cellular neurosciences*
856 37:284–97. DOI: 10.1016/j.mcn.2007.10.003.

857 Yu X, Jin L, Zhang X, Yu X. 2013. Effects of maternal mild zinc deficiency and zinc
858 supplementation in offspring on spatial memory and hippocampal neuronal ultrastructural
859 changes. *Nutrition (Burbank, Los Angeles County, Calif.)* 29:457–61. DOI:
860 10.1016/j.nut.2012.09.002.

861 Yu X, Ren T, Yu X. 2013. Disruption of calmodulin-dependent protein kinase II α/brain-derived
862 neurotrophic factor (α-CaMKII/BDNF) signalling is associated with zinc deficiency-
863 induced impairments in cognitive and synaptic plasticity. *The British journal of nutrition*
864 110:2194–200. DOI: 10.1017/S0007114513001657.

865

866

867

868

Figure 1

Cerebral organoids derived from human embryonic stem cells.

(A) Sequential steps involved in the generation of cerebral organoids from human pluripotent stem cells. (B) Spheroid cerebral organoids of 45-days old presenting smooth texture and homogeneous coloring. (C and C') Microphotography of a 30-days old organoid in detail showing distinct hues according to different cell layers. (D) Organoid diameter quantification; organoids were measured at different stages of the differentiation process. Organoids' diameter doubled between days 7 and 15 in culture and quintupled after 45 days. The graph represents mean ± S.D. n=107 for 7-days old organoids, n=90 for 15-days old organoids, n=56 for 30-days old organoids, n=18 for 45-days old organoids. ***p < 0.0001 for 7-days old versus 15, 30 and 45-days old organoids. Cerebral organoids were obtained from two independent assays. Scale bars: B = 1 mm, C = 125 µm and C' = 25 µm.

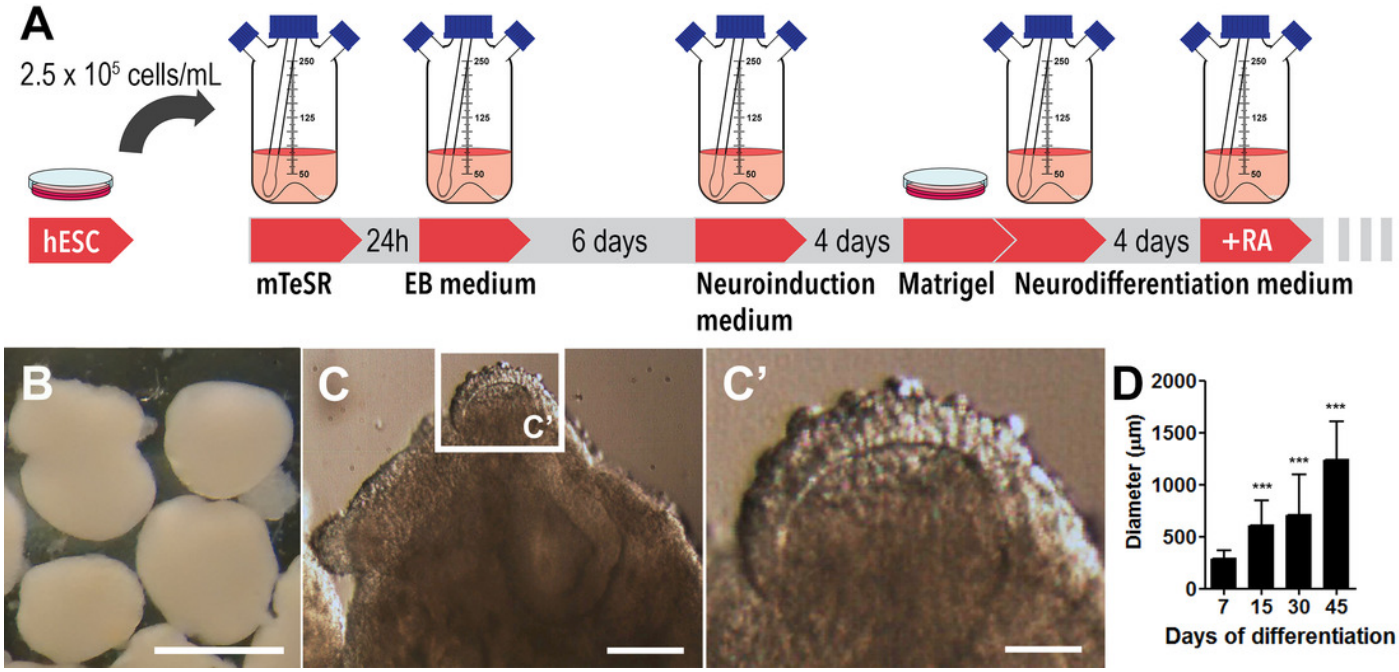

Figure 2

Cerebral organoids present epithelium-lined cavities morphologically similar to ventricles.

(A) Within 30 days of differentiation, cerebral organoids formed large cavities morphologically similar to ventricles, lined with stratified epithelium (A'). (B) After 45 days of differentiation, the lumens of these cavities seemed flattened and (B') the surrounding epithelium length seemed reduced. (A, A', B, and B') H&E staining. (C) Measurements of the putative ventricles showed a reduction in average luminal area. (D) Concomitantly, the number of epithelium-lined cavities per cerebral organoid tissue section was reduced from 30 to 45 days of differentiation. The graphics represent mean ± S.D. Luminal area measurements: n=17 for 30-days old organoids and n=09 for 45-days old organoids. Number of putative ventricles per organoid: n=6 for 30-days old organoids and n=11 for 45-days old organoids, *$p < 0.05$. Cerebral organoids were obtained from two independent assays. Scale bars: A and B = 100 µm, A' and B' = 50 µm.

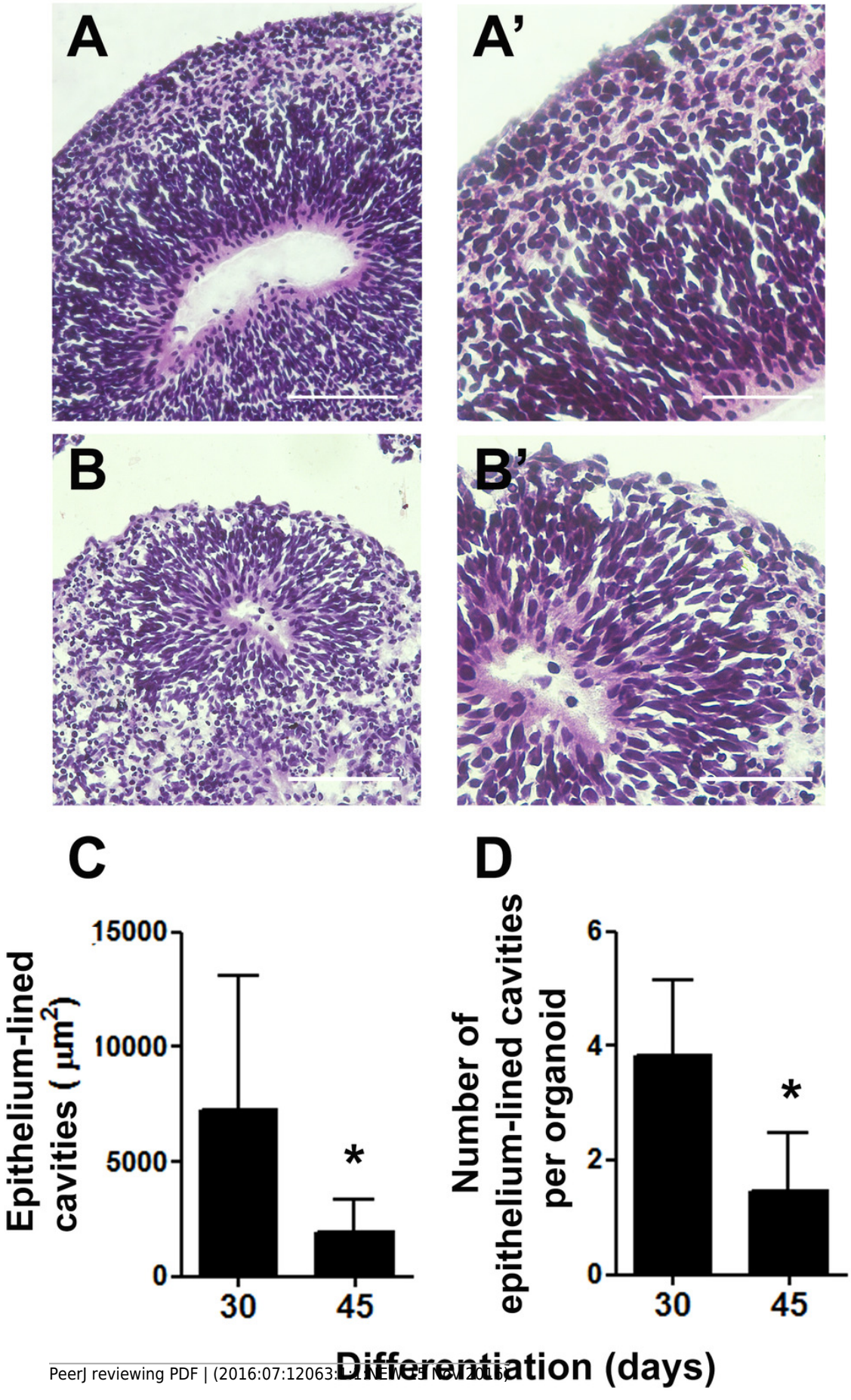
A
A'
B
B'
C
D
Epithelium-lined cavities (µm²)
15000
10000
5000
0
30
45
*
Number of epithelium-lined cavities per organoid
6
4
2
0
30
45
*
Differentiation (days)

Figure 3

Cerebral organoid cytoarchiteture after 30 and 45 days in culture.

In 30-days old organoids, (A) positive cells for the intermediate filament nestin were observed throughout cerebral organoids' extension. (B) The luminal surface of the epithelium-lined cavities was populated by mitotic cells (PH3), (C) identified as apical progenitors (PAX6) in the ventricular zone. (D) Intermediate progenitors expressing TBR2 were also present in the ventricular zone and composed an adjacent layer, the subventricular zone. (C and D) Tangential migratory neurons (β-tubulin III and MAP2) established the pre-plate outside germinal zones. In 45-days old organoids, (E) the flattened ventricles still presented proliferative cells (Ki67 and PH3) and (F) neural progenitors (TBR2) in the radially organized cell layer. (G) MAP2 positive cells were found widespread, except in germinal zones, while GAD67 (GABA synthesis enzyme) positive cells (H) or the neurotransmitter glutamate (I) became evident. In this time point, synaptic markers such as synaptophysin and PSD95 (J) were also observed. Finally, comparing 30 to 45-days old cerebral organoids, there was a reduction in the number of PH3 positive cells (K), while the neuronal population was expanded (L) as well as neurons producing GABA (M) or cells producing glutamate (N). Graphics are represented as mean ± S.D. For 30-days old and 45-days old organoids, respectively: PH3 positive cells, n=3 and n=5; MAP2 positive area, n=4 and n=6; GAD67 positive cells, n=2 and n=4; glutamate fluorescence intensity, n=6 and n=7, *$p<0.05$. Scale bars: A, B, F, G = 100 µm; C, D, E, H, J = 50 µm.

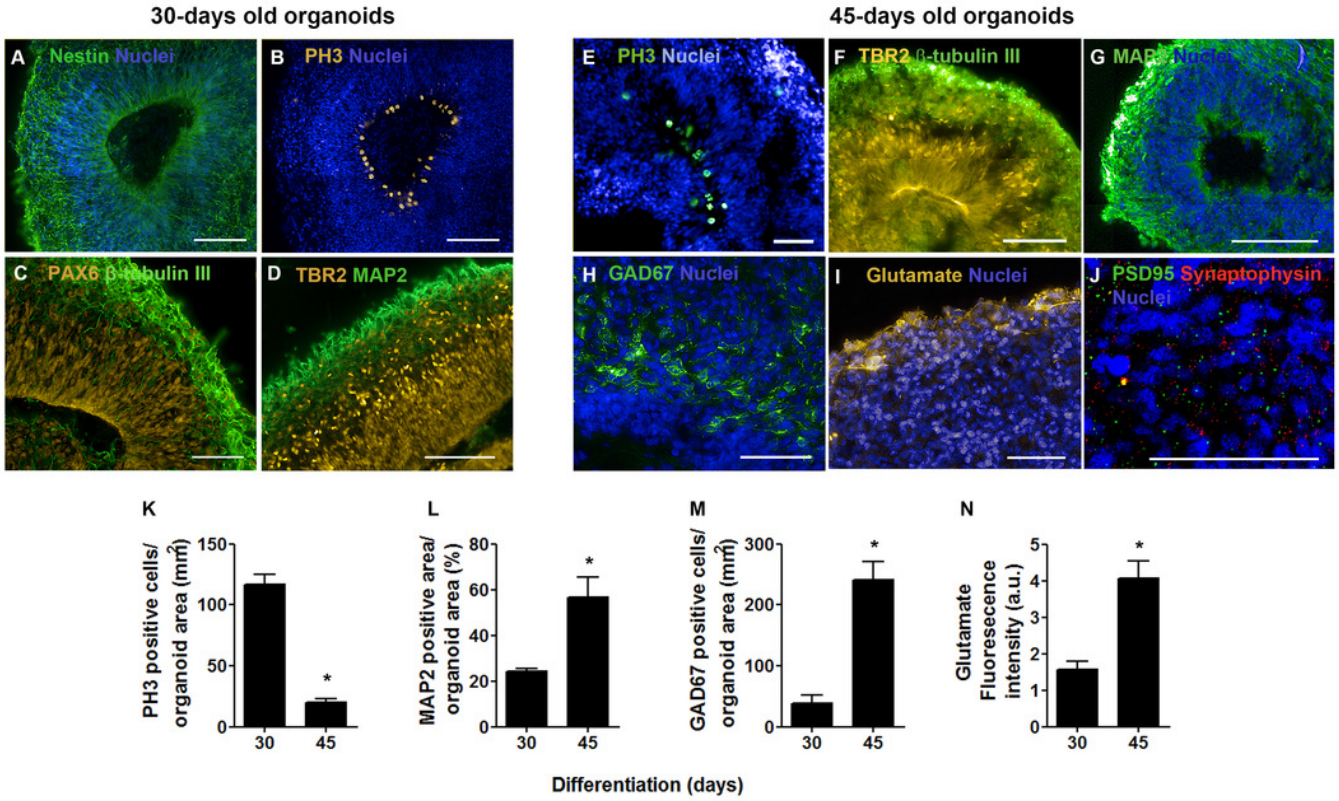
30-days old organoids
45-days old organoids
A Nestin Nuclei
B PH3 Nuclei
C PAX6 β-tubulin III
D TBR2 MAP2
E PH3 Nuclei
F TBR2 β-tubulin III
G MAP2 Nuclei
H GAD67 Nuclei
I Glutamate Nuclei
J PSD95 Synaptophysin Nuclei
K
PH3 positive cells/ organoid area (mm²)
150
100
50
0
30
45
*
L
MAP2 positive area/ organoid area (%)
80
60
40
20
0
30
45
*
M
GAD67 positive cells/ organoid area (mm²)
300
200
100
0
30
45
*
N
Glutamate Fluoresecence intensity (a.u.)
5
4
3
2
1
0
30
45
*
Differentiation (days)

Figure 4

Elemental distribution in cerebral organoids.

Representative color gradient heat maps of 30 and 45-days old cerebral organoids. Elemental maps revealed diffusion patterns for P, S, K, Ca, Fe and Zn. Scales correspond to weight fraction units (ppm or µg/g = weight fraction*10^6).

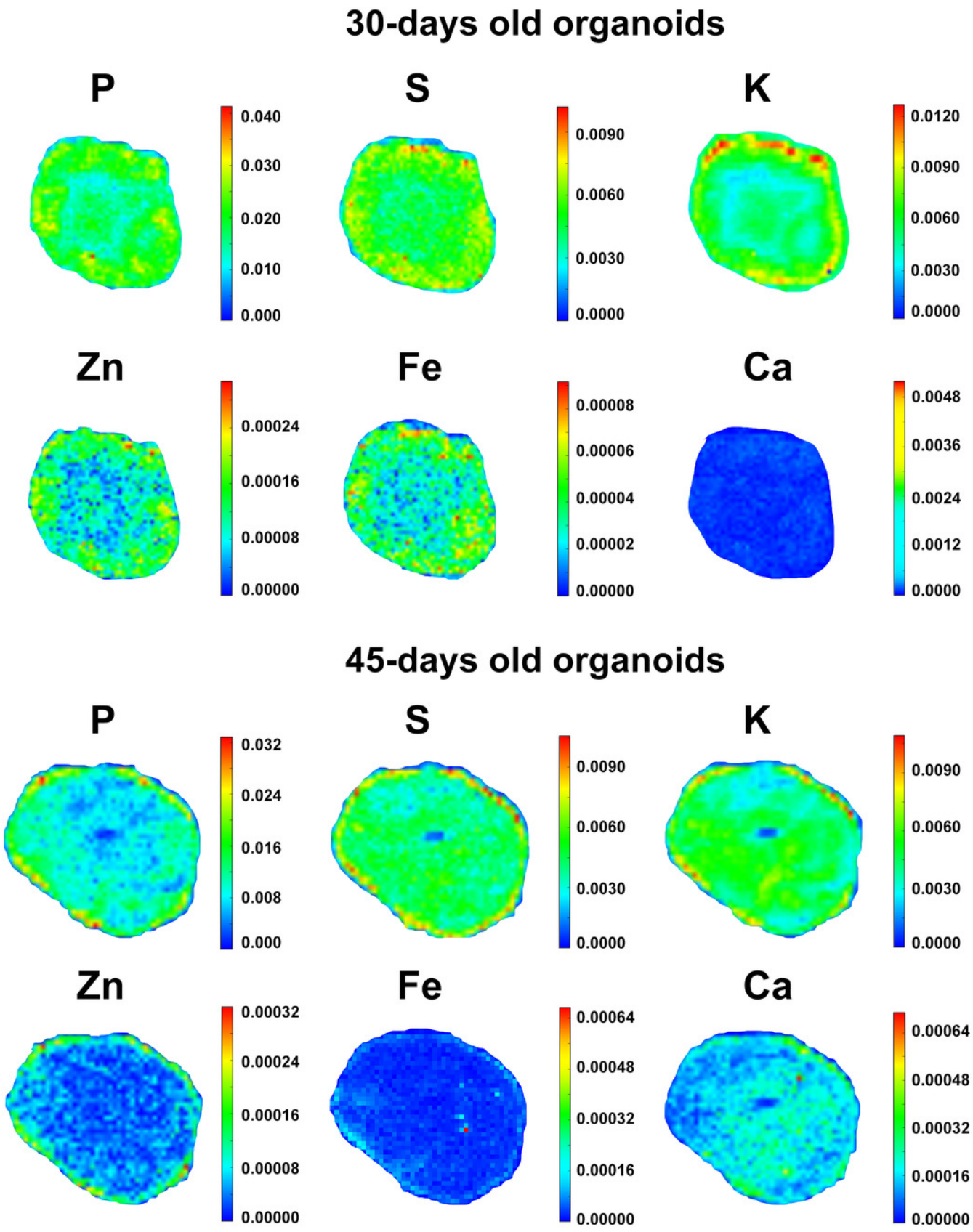
30-days old organoids
P
0.040
0.030
0.020
0.010
0.000
S
0.0090
0.0060
0.0030
0.0000
K
0.0120
0.0090
0.0060
0.0030
0.0000
Zn
0.00024
0.00016
0.00008
0.00000
Fe
0.00008
0.00006
0.00004
0.00002
0.00000
Ca
0.0048
0.0036
0.0024
0.0012
0.0000
45-days old organoids
P
0.032
0.024
0.016
0.008
0.000
S
0.0090
0.0060
0.0030
0.0000
K
0.0090
0.0060
0.0030
0.0000
Zn
0.00032
0.00024
0.00016
0.00008
0.00000
Fe
0.00064
0.00048
0.00032
0.00016
0.00000
Ca
0.00064
0.00048
0.00032
0.00016
0.00000

Figure 5

Elemental quantification in cerebral organoids.

Cerebral organoid elemental composition was also assessed by SR-XRF. Scatter plots represent values found for each sample. (A) P, *p=0.036; (B) S, p=0.22; (C) K, *p=0.0461; (D) Ca, p=0.6696; (E) Fe, p=0.08; (F) Zn, ***p<0.0001. PPM=parts per million.

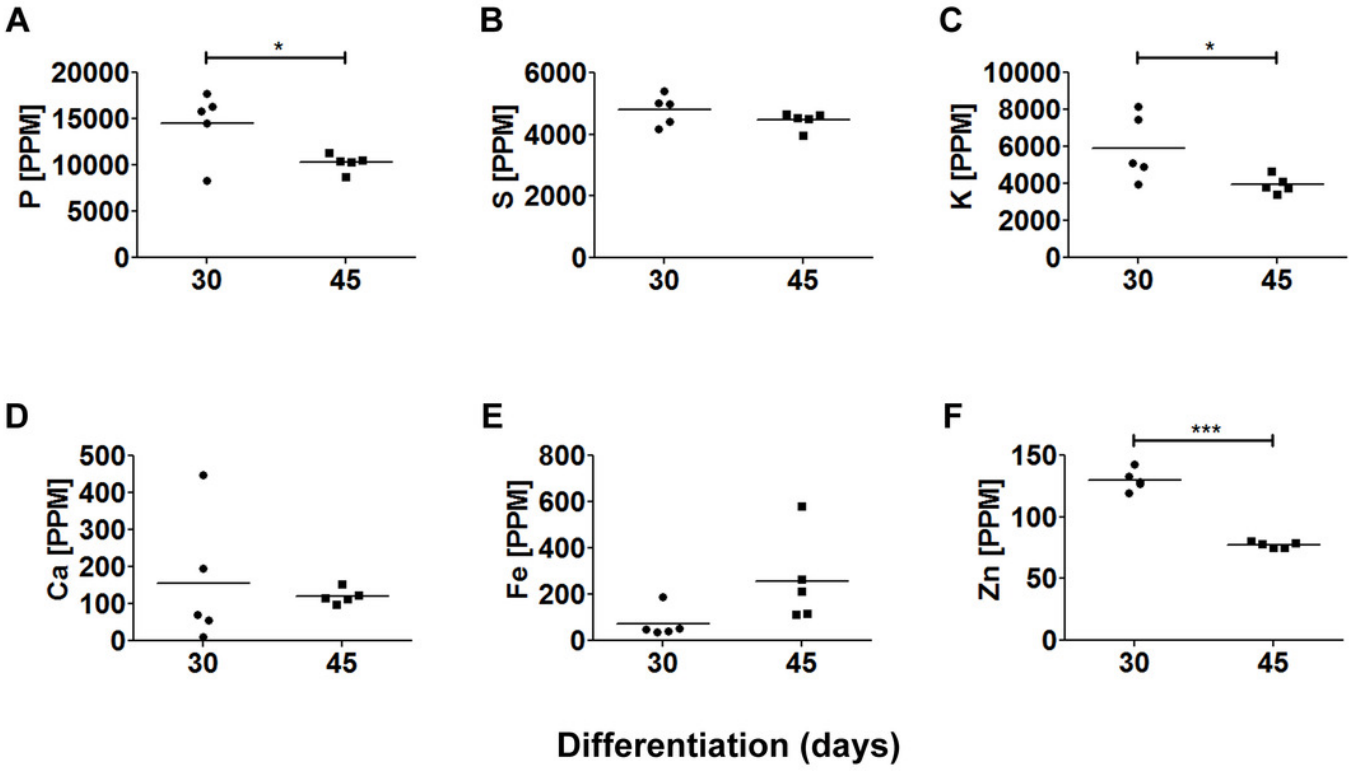

Figure 6

Concentration gradient heat maps overlay for elemental colocalization in cerebral organoids at 30 and 45-days of development.

Representative merged color-gradient maps of organoids' elements pairs: P/S at 30 (A) and 45 (D) days of differentiation; P/Zn at 30 (B) and 45 (E) days of differentiation; K/Ca at 30 (C) and 45 (F) days of differentiation. Elements are represented in: P (red), S (green), K (blue), Ca (red) and Zn (blue).

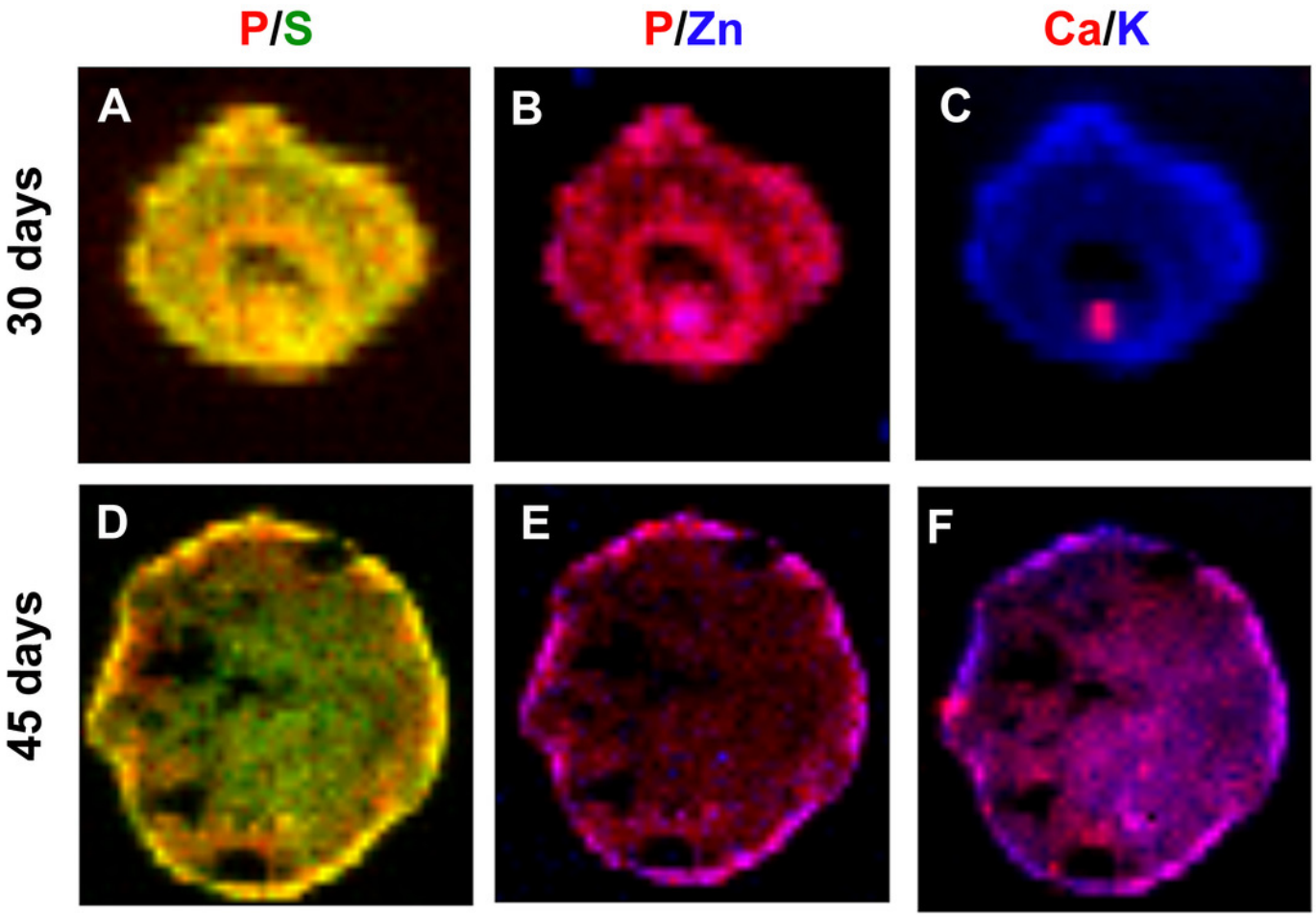

Table 1(on next page)

Trace elements detected in cerebral organoids and its corresponding functions in the brain development.

1

Element	Cellular function	Role in brain development	References
P	• Nucleoproteins • Phospholipids • ATP	• Neurogenesis (cellular membrane biogenesis)	Silvestre, Maccioni & Caputto, 2009
S	• Protein synthesis • Cysteine • Disulfide bonds	• Neurogenesis • Neuronal migration (proteoglycans and glycosaminoglycans) • Axon guidance	Inatani et al., 2003; Girós et al., 2007; Maeda, 2015
K	• Protein synthesis • RNA synthesis • Cell division • Transmembrane transport	• Resting potential • Neurogenesis • Neural progenitors' survival	Lubin & Ennis,1964; Schaarschmidt et al., 2009
Ca	• Cell signaling • Enzymatic cofactor • Regulation of gene expression • Cell motility	• Neurogenesis • Neuronal differentiation • Release of synaptic vesicles	Weissman et al., 2004; Shin et al., 2010; Resende et al., 2010; Atlas, 2013
Fe	• DNA synthesis • Lipid synthesis • Energetic metabolism • Metalloproteins	• Neurogenesis • Neuronal differentiation • Monoamine metabolism • Modulation of dopaminergic receptors • Synaptic maturity • Myelin synthesis	Erikson et al., 2001; VanLandingham & Levenson, 2003; Lozoff & Georgieff, 2006; Tran et al., 2008
Zn	• Protein synthesis • DNA synthesis • Zinc finger transcription factor • Metalloproteins	• Neurogenesis • Neuronal differentiation • Synaptic modulation • Dendritic arborization • Myelin synthesis	Liu et al., 1992; Gao et al., 2009; Levenson & Morris, 2011; Morris & Levenson, 2013; Marger, Schubert & Bertrand, 2014

2

3

Table 2(on next page)

Elemental correlation analysis for pairs of elements.

Pearson’s product-moment correlation coefficient (Pearson’s r) and R-squared from lines of best fit were calculated for each elemental pair in order to reveal correlated and uncorrelated pairs. A 45 days/30 days old organoids ratio was calculated in order to highlight time-dependent changes in elements' correlational distribution. Data are represented as mean ± S.D. For 30-days old cerebral organoids, n=4 and for 45-days old cerebral organoids, n=5. For all correlations of element pairs, p<0. 05; except for one 30-days old cerebral organoid in the analysis of K/Fe pair and one 45-days old cerebral organoid in the analyses of K/Fe and P/Fe pairs.

1

Compared elements (pairs)	Pearson's r			R-squared		
	30 days (mean ± SD)	**45 days** (mean ± SD)	**45/30 days** (ratio)	**30 days** (mean ± SD)	**45 days** (mean ± SD)	**45/30 days** (ratio)
P/S	0.9607 ± 0.0078	0.9266 ± 0.0097	0.96	0.9231 ± 0.0149	0.8587 ± 0.0180	0.93
P/K	0.8345 ± 0.0826	0.8922 ± 0.0112	1.07	0.7016 ± 0.1363	0.7962 ± 0.0199	1.13
P/Ca	0.1927 ± 0.1791	0.5509 ± 0.2528	2.86	0.0612 ± 0.0810	0.3546 ± 0.2263	5.79
P/Fe	0.4294 ± 0.4468	0.3942 ± 0.3071	0.92	0.3341 ± 0.3689	0.2309 ± 0.2449	0.69
P/Zn	0.8365 ± 0.0385	0.7331 ± 0.0467	0.87	0.7008 ± 0.0644	0.5391 ± 0.0664	0.77
S/K	0.8490 ± 0.0794	0.9358 ± 0.0157	1.10	0.7256 ± 0.1315	0.8759 ± 0.0292	1.21
S/Ca	0.1851 ± 0.1592	0.5951 ± 0.2744	3.21	0.0532 ± 0.0665	0.4144 ± 0.2662	7.79
S/Fe	0.4386 ± 0.4522	0.5000 ± 0.2286	1.14	0.3457 ± 0.3811	0.2892 ± 0.2317	0.83
K/Ca	0.1484 ± 0.1225	0.5979 ± 0.2638	4.03	0.0333 ± 0.0404	0.4132 ± 0.2649	12.41
K/Fe	0.2944 ± 0.3534	0.4018 ± 0.2987	1.36	0.1551 ± 0.2437	0.2283 ± 0.2294	1.47
K/Zn	0.7137 ± 0.0674	0.6493 ± 0.0777	0.91	0.5128 ± 0.0968	0.4265 ± 0.0989	0.83
Ca/Zn	0.3459 ± 0.1044	0.4256 ± 0.1003	1.23	0.1278 ± 0.0744	0.1891 ± 0.0784	1.48
Fe/Zn	0.5114 ± 0.3433	0.4445 ± 0.1812	0.87	0.3500 ± 0.3418	0.2239 ± 0.1791	0.64

2

3

4

5